Submitted to Annals of Glaciology, **59A80** *31 August 2010*

The triggering of sub-glacial lake drainage during rapid glacier drawdown: Crane Glacier, Antarctic Peninsula

Ted A. Scambos[1], Etienne Berthier[2], and Christopher A. Shuman[3]

[1]*National Snow and Ice Data Center, University of Colorado, Boulder CO 80309, USA*

[2] *CNRS; Université de Toulouse ; LEGOS; 14 Av. Ed. Belin, 31400 Toulouse, France*

[3] *Goddard Earth Science and Technology Center, University of Maryland-Baltimore County, NASA Goddard Space Flight Center, Greenbelt MD 20771 USA*

Corresponding author: T. Scambos, teds@nsidc.org; 303 492-1113

Abstract. Ice surface altimetry from ICESat-1 and NASA aircraft overflights spanning 2002 to 2009 indicate that a region of the lower Crane Glacier shows an unusual temporal pattern of elevation loss: a period of very rapid drawdown (~91 ma^{-1} between September 2004 and September 2005) bounded by periods of more moderate rates (23 ma^{-1} until September 2004; 12 ma^{-1} after September 2005). The region of increased drawdown is 4.5 by 2.2 km, ~6 km^2, based on satellite (ASTER and SPOT5) stereo-image DEM differencing spanning the event; in a later differential DEM the anomalous drawdown feature is not seen. Bathymetry in Crane Glacier fjord reveals a series of flat-lying, formerly sub-glacial deeps, downstream of the feature, interpreted as lake sediment basins. Our conclusion is that the elevation change feature resulted from drainage of a small, deep sub-glacial lake. Airborne laser altimetry and satellite-derived DEM show that mean longitudinal slope over the feature increased prior to the drainage event, from 0.026 (±0.002) in November 2002 to 0.033 (±0.002) in November 2004, and near zero by November 2008. We infer that the drainage event was induced by hydraulic forcing of sub-glacial water past a downstream obstruction to drainage. Ice dynamics and edge effects make it likely that the size of the lake was smaller, but deeper, than its surface expression. However, only a fraction of Crane Glacier's increase in flow speed that occurred near the time of lake drainage appears to be directly attributed to the event; instead, retreat of the ice front off a sub-glacial ridge 6 km downstream of the lake is likely the dominant cause of a return to strongly negative mass balance in the past 4 years.

(277 words)

Keywords: Sub-glacial lakes, Crane Glacier, laser altimetry, glacier mass balance.

1 Introduction

A resurgence of interest in sub-glacial hydrology, particularly in the Antarctic ice sheet system, has been sparked by the recent successes of satellite altimetry and interferometric SAR in detecting subtle, localized elevation changes. These are interpreted as active, volume-changing sub-glacial lakes interconnected by drainage systems (Remy and Legresy, 2004; Gray et al., 2005; Wingham and Shepherd, 2006; Fricker et al., 2007; Stearns et al., 2008; Fricker and Scambos, 2009). Hundreds of these active sub-glacial systems have now been identified (Smith et al., 2009), and in one case at least, they are shown to have an effect on ice flow (Byrd Glacier, Stearns et al., 2008). Moreover, compendia of both radar reflection evidence and surface morphological indicators of larger sub-glacial water bodies (Siegert et al., 2005; Smith et al., 2009) show that not only are these also widespread, but that they, too can have important effects on ice flow (e.g., Bell et al, 2006).

Despite these advances, a class of sub-glacial water bodies remains largely unmapped; smaller pockets (< a few ice thicknesses across) that remain stable. Since these features may not have a surface elevation change over time associated with them (which permits detection), and do not affect surface morphology significantly, they are detectable only by radio-echo surveys, which are sparsely distributed. In the case of heavily crevassed outlet glaciers, such as for the case here, it may be difficult to detect the sub-glacial water body with radio-echo surveys. Recent modeling studies of sub-glacial melt rates (Pattyn, 2010), and the obvious irregularity of both the surface topography and bed elevation, where mapped in detail (e.g., West Antarctica: Shabtaie and Bentley, 1988; and http://www.ig.utexas.edu/research/projects/agasea; East Antarctica: Bo et al., 2009; and http://www.ldeo.columbia.edu/~mstuding/AGAP/AGAP_GAMBIT_maps.html) show that abundant sub-ice water is available and that there are numerous places where it may be trapped. As our ability to map the base of the ice sheet and detect the presence or absence of sub-glacial water bodies

improves, it is likely that we will find an ice sheet bed surface as pocked with lakes as the current land areas that were formerly beneath ice sheets (e.g., the Canadian Shield and Scandinavia; Clarke, 2005).

These small stable water bodies, if widespread, represent an important additional potential contributor to mass balance changes as a glacier responds to climate-driven changes in flow. In the case of retreating tidewater glaciers, as glacier mass imbalance increases, the surface slope generally increases. Changes in surface slope across a sub-glacial body of water must create sub-glacial pressure gradient changes, forcing the water to move toward the downslope direction. The trapping mechanism that sustained the lake (bedrock sill, sediment plug, or a local high in sub-glacial hydraulic potential) is tested, and if pressure changes are great enough, it is breached. The water drains into the sub-glacial environment downstream.

At Crane Glacier, an outlet glacier draining the eastern Antarctic Peninsula, we have mapped a case where such an ice dynamics-driven (more broadly, climate-driven) slope change has apparently caused a moderate-volume sub-glacial water pocket to be forced to drain into the sub-glacial environment (Figure 1). Crane Glacier is the largest of the outlet glaciers flowing into the embayment created by the loss of the Larsen B ice shelf in February-March of 2002 (Scambos et al., 2003). Response of the several glaciers affected by the loss was an almost immediate acceleration in flow speed, rising to 6 – 8 times the pre-shelf-loss speed by late 2003 (Rignot et al., 2004; Scambos et al., 2004). However, beginning in early 2004, Crane Glacier slowed significantly, to just twice the pre-breakup speed, before re-accelerating in 2005 (Hulbe et al., 2008). Shuman et al. (2010) discuss the regional elevation response since shelf break-up, and identify that the Crane Glacier trunk has an anomalously large and spatially extensive response in recent years relative to adjacent similar glaciers. As developed below, the anomalous elevation loss event in the lower trunk of the glacier occurred simultaneously with a renewed ice acceleration.

In the following text we compile evidence from satellite and airborne laser altimetry, satellite stereo-image DEMs, and image pair velocity maps to examine the sudden elevation loss event and its effects on ice flow. To date, no reliable bed data from radio echo surveys exist for lower Crane Glacier. Bathymetry of the Crane Glacier fjord (E. Domack, personal communication, Mueller et al. 2006, and Rebesco et al., 2010 submitted; Figure 1) and other sources, combined with the observations of abrupt elevation change, support a model of drainage of a sub-glacial lake for the event. However, retreat of the glacier front from a bedrock high in the fjord, as mapped by the bathymetry, also played a role in the glacier evolution at the time of the inferred lake drainage event. We compare the significance of the lake drainage and ice front retreat on ice flow and mass balance for Crane Glacier, and thereby gain insight into the importance of a potential sub-glacial water feedback on retreating outlet glaciers.

2 Data Sources and Methods

The Ice, Cloud, and land Elevation Satellite (ICESat, which we will call ICESat-1 to distinguish it from the upcoming ICESat-2 sensor and satellite system) provided global elevation mapping below 86° latitude between 20 February 2003 and 11 October 2009. ICESat-1 carried an orbiting infrared (1064 nm) pulse-laser system that acquired ranging times to the surface (or intervening cloud or aerosol layers) at a 40 Hz rate, roughly equivalent to 172 m ground spacing (Zwally et al., 2002; Shutz et al., 2005). Spot size of the laser pulse on the ground was nominally 70 m, although the majority of the data was acquired with a 50 m footprint. The spacecraft was flown in both 8-day and 91-day repeat track orbits, and the majority of the data was collected in a 33-day sub-cycle of the 91-day orbit. One orbit track (Track 0018) crossed the lower Crane Glacier. Out of 16 total track acquisitions of 0018 over Crane Glacier, useful ice surface data were acquired on 10 of them (6 near-complete profiles, and 4 partial profiles). Error of the ICESat-1 elevation measurements over flat snow-covered terrain is approximately 20 cm (Shuman et al., 2006). Shot-to-shot variations and small-scale differences between repeated profiles suggest an

error of 2 to 3 meters over the extremely rough ice of lower Crane glacier (which has sub-laser-spot scale crevassing and seracs, especially after 2004). ICESat-1 data may be acquired from the National Snow and Ice Data Center (http://nsidc.org/data/icesat).

NASA has operated an airborne laser altimetry system, the Airborne Topographic Mapper, for surveys of ice sheets, glaciers, sea ice and other land and ocean areas since 1991 (Krabill et al., 1995; Abdalati and Krabill, 1999). There have been multiple versions and software adjustments over time, but the basic system remains a helical-scanning pulse laser, operating at 532 nm (frequency-doubled from a 1064 nm laser source) with a laser pulse rate of 3 kHz. The laser pulses produce a set of dense, overlapping elliptic helical tracks of surface measurements that are processed into along-flight tracks of 'plates', i.e. mean slope and elevation values extracted from the full data set at 70 x 70 m intervals on either side of the flight line (4 or 5 plates across-track, continuous along-track). Errors for the 70 x 70 m mean slope and elevation grid cells are a few centimeters under optimum conditions but can be as large as several decimeters (Krabill et al., 1995; Thomas et al., XXXX). Overflights of the Crane Glacier trunk by the ATM system have occurred on 26 November 2002, 29 November 2004, and 21 October 2008. (A more recent flight in November, 2009 was not available as of this writing.) The 2008 profile did not cross the same point on ICESat track 0018 (see Figure 1), and so a local simple geometric correction was applied to estimate the height at the intersection of the 2002 and 2004 ATM data and the ICESat Track 0018 on that date. ATM data is available from the National Snow and Ice Data Center's Ice Bridge project (nsidc.org/data /icebridge) and from the University of Kansas Center for the Remote Sensing of Ice Sheets (CReSIS: www.cresis.ku.edu).

We also generated a series of digital elevation models (DEMs) of the Crane Glacier trunk and nearby glaciers, based on satellite stereo digital images (Table 1). We used 6 such stereo-image DEMs in evaluating the topographic evolution of the lower Crane Glacier. The two sensors used are the Advanced Spectral and Thermal

Emission Radiometer (ASTER) flying on NASA's Terra platform, and SPOT-5, the fifth satellite of the Systeme Pour l'Observation de la Terre (SPOT) series. Both these satellites acquire along-track stereo pair imagery by a fore and aft (or nadir and aft) acquisition scheme. The systems have imagery with 15 and 5 m resolution, respectively, and under ideal conditions can resolve elevations to approximately 5 m (Bouillon et al., 2006; Fujisada et al., 2005; Toutin, 2008). However, problems with sky clarity, snow/ice reflectance variations, and extreme surface roughness at the pixel scale can reduce this accuracy to a few 10s of meters (Berthier and Toutin, 2008), creating elevation 'noise' over short distances (2-5 pixels). In general the profiles are precise (±5 m) at averaging scales above 10 pixels. Profiles from the satellite stereo DEMs were extracted along the track of the airborne altimetry, providing greater temporal resolution of along-flow slope changes, albeit with greater vertical 'noise' than the altimeter data.

ASTER and SPOT-5 DEMs are automatically derived from stereo-imagery without ground control points and, thus, may contain altimetric biases up to 15 m (Berthier et al., 2010). For the 25 November 2006 SPOT-5 DEM, those biases have been estimated and corrected using ICESat-1 data acquired during laser period 3G, just 10 day before the acquisition date of the SPOT-5 stereo pair. For each ICESat footprint, the corresponding SPOT-5 DEM elevation was extracted by bilinear interpolation. A vertical bias of 3 m (standard deviation 5.5 m, N=558) was corrected. Next, all other satellite DEMs were vertically adjusted to the 25 November 2006 SPOT-5 reference DEM by minimizing the elevation differences on the (assumed) stable regions outside of the fast changing outlet glaciers.

Near-infrared and visible band images from several sensors were used to create a series of ice velocity mappings of lower Crane Glacier by an image-to-image correlation technique (Bindschadler and Scambos, 1991). We use software available at the NSIDC website (IMCORR, at http://nsidc.org/data/velmap/software.html; see Scambos et al., 1992) except for the December-2009 to January-2010 SPOT-5 velocity field, which was created using the MEDICIS software (Berthier et al., 2005).

Six image pairs are used to map the flow speed in a small region near the intersection of the ATM and ICESat-1 0018 tracks and two pairs are used to map ice flow before and after the rapid drawdown over a broader region of the lower glacier trunk (Table 1). Errors in the flow speed measurement for an image pair are a function of image co-registration accuracy, image cross-correlation precision, and the time between the image acquisitions. Image correlation precision is 0.25 pixels for each high-confidence correlation match. Image coregistration error ranges from ~1 pixel for Landsat-7, ~1 pixel for ASTER, and ~0.5 or less for SPOT-5 images.

3 Observations

Bathymetry data shown in Figure 1 were collected from the *RV Nathaniel B. Palmer* in March-April of 2006 using a multi-beam sonar system (Mueller et al., 2006; Rebesco et al., 2010 submitted, and E. Domack, personal communication). Maximum fjord depth at the ice front was 1220 m. The glacier front at that time was afloat, with approximately 300 meters of water depth below the ice at the center of the ice front. Bathymetric mapping of the seaward portion of the fjord reveals a series of low basins (labeled 1, 2, and 3 in Figure 1). These basins have smooth flat-lying surfaces and layered sediments and are interpreted as sub-glacial sediment ponds, i.e. sub-glacial lake deposits (Rebesco et al., 2010 submitted). Between the submerged lake basins are significant bathymetric ridges, rising to 950 m depth between basins 2 and 3. Ice fronts positions digitized from Landsat-7, ASTER, and SPOT5 images used in the velocity mapping (described below) show that the ice front lay near this ridge in late September 2004, just prior to significant elevation and flow speed changes. It subsequently retreated during late 2004 and 2005, approximately 2 km, to a position that it has more or less maintained for the past several years (see http://nsidc.org/agdc/iceshelves images for a detailed series of satellite images covering the region).

A history of elevation over time (December 2001 to late 2009) for the region of the intersection of ICESat-1 track 0018 and the ATM near-centerline glacier profiles (65.35°S, 62.45°W) highlights the anomalous elevation loss rate and magnitude at

that site between September 2004 and September 2005 (Figure 2). The disintegration of the Larsen B ice shelf precipitated large changes at the Crane glacier front, and a near-immediate acceleration of the lowermost glacier (Scambos et al. 2004); however, elevation change did not begin at the point of the intersection until sometime after December 2002. The site is 12.3 km upstream from the pre-breakup grounding line (Rack and Rott, 2004). Following that time, elevation loss appears to have been steady at a rate of about 23 ma^{-1} until September 2004. A closely spaced series of elevation measurements at the site constrain the onset of increased drawdown rate to be near this time, and abrupt. Over the next year, the rate of elevation loss averaged 91 ma^{-1}, ending in late September 2005 or possibly slightly before. Following September 2005, elevation loss occurred at 12 ma^{-1}. As of this writing, it appears that the elevation loss rate has slowed or even reversed, beginning sometime in 2009. (The elevation increase shown in the preliminary November 2009 LVIS data will be checked against 2009 ATM and LVIS data when available, prior to publication).

Satellite stereo-image DEMs allow us to examine elevation changes more regionally. A differencing of DEM mappings based on images acquired just prior to increased drawdown (27 Sep. 2004 ASTER), just after (01 Jan. 2006), and well after (25 Nov. 2006) allows us to examine the regional extent of the abrupt elevation change at the ATM/ICESat 0018 intersection (Figure 3) over the lower Crane Glacier. Differencing of the September 2004 and January 2006 DEMs indicate that the region of abrupt, anomalous elevation change is quite localized, and was several tens of meters greater than the loss in the surrounding regions. An outline of a region tracing the maximum gradient in the anomaly encloses a region 1.9 by 1.5 km. A later difference DEM using the January 2006 SPOT5 data and a November 2006 SPOT5 elevation map shows no evidence of the anomaly region; rather, elevation loss appears to be nearly uniform over the lower trunk, at ~20 m loss over the interval.

Slope changes along the glacier centerline over the elevation change anomaly provide some insight into the timing and causes of the abrupt elevation loss (Figure

4). First, differencing elevation profiles from before and after the period of rapid elevation loss (ASTER 7 November 2002 and SPOT-5 1 January 2006) indicate a 4.5 km total extent of the region of anomalous elevation loss, with a maximum of 40 meters additional loss relative to areas upstream (98 m loss) and downstream (103 m loss; see Figure 4 inset). The 4.5 km along-flow region spanning the anomalous elevation loss area shows a slightly increasing surface slope through time, from 0.020 in November 2001 (ASTER DEM prior to shelf breakup), to 0.026 in November 2002 (ATM profiles) as the post-shelf break-up effects propagate up-glacier. Slope across the region remains near that value in ASTER DEM longitudinal profiles in January 2004 (0.026) and September 2004 (0.024) that immediately precede the rapid elevation loss. The ATM profile of November 2004 shows an increased slope, to 0.033, at the onset of rapid elevation loss. Data from 2006 and later show much lower slopes, and a significantly changed profile. The October 2008 mean slope is 0.001. The ATM slope profiles track the development of the surface basin on the glacier, and confirm the changes seen in DEM differencing.

A very large renewed acceleration of the glacier occurs at the same time (within months) of the sudden elevation loss over the anomaly and retreat of the ice front from the bedrock high (Figure 5). Speed of the glacier at this site increases rapidly after loss of the ice shelf in early 2002, peaking at 710 ma^{-1} in early 2003. Pre-shelf breakup speed in this region of the glacier has been estimated at 300 ma^{-1}, (Rignot et al., 2004). By late 2003, the glacier begins to slow again, to near 470 ma^{-1} (Figure 5; see also Hulbe et al., 2008).

Attempts to use image correlation of image pairs straddling the period of anomalous elevation loss and the last stage of ice front retreat to measure ice velocity failed because the glacier surface undergoes a large change during this period, dramatically increasing the density and intensity of crevassing. This change occurs over the entire lower trunk of the glacier (Figure 6). In the SPOT-5 image pair used here just after the lake drainage event (January 2006 and November 2006, see Table 1), a very large increase in speed is measured, roughly 4 times the pre-elevation loss

(and pre- front retreat) speed (to 1943 ma^{-1}; Figure 5). By early 2009, this decreased to 1430 ma^{-1}, as measured by a Formosat-2 image pair (Scambos and Liu, 2009). A SPOT-5 image pair acquired in late 2009 and early 2010 yielded a speed of 1270 ma^{-1} in the anomaly region.

As noted above, in the months following the elevation change that began in September 2004, the glacier develops a dense crevasse network for the 10 km just upstream from the ice front (Figure 6). Prior to this time, the glacier surface is relatively uncrevassed and gently undulating (Figure 6a and 6b), despite the fact that it had already accelerated by a factor of 3 to 6 in the aftermath of the Larsen B Ice Shelf disintegration. The surface character is essentially unchanged between November 2002 and September 2004. As the anomalous elevation loss and most recent significant ice front retreat begins in late 2004, the surface becomes covered in a dense network of crevasses at several orientations. This is particularly the case in the lowermost 2 km of the central glacier trunk, where the ice was observed to be afloat in 2006 (see Figure 1), but the new dense crevasse pattern extends well upstream of the anomalous elevation loss region. This new surface character persists through 2006 (Figure 6c and 6d) and is observed at present.

To examine the potential causes of the secondary (2004-2006) large acceleration and crevasse changes, we further analyzed the ice flow speed of a larger area of the lower Crane Glacier trunk using the best image pairs available (i.e., broadest clear-sky coverage) from the Figure 5 analysis. The selected image pairs for speed analysis in Figure 6 are given in Table 1. Figure 6b contains contours from the December 2002 - February 2003 image pair. While this pair had a higher potential error for a single vector, the image features correlated very well, providing a dense vector field (~4500 vectors) that reduced the uncertainty of the velocity measurement (smoothing the grid by an inverse square algorithm with 600 x 600 m regions containing an average of 16 vectors each reduced the error reported in Table 1 by a factor of 4). The 6b contours show that acceleration of the glacier in the aftermath of the 2002 Larsen B shelf disintegration was broad and uniform, with

little evidence of local variations in basal or lateral shear. The longitudinal gradient in velocity is relatively constant. The 2006 image pair yielded fewer, less uniformly distributed vectors (2340 vectors) due to a rough surface and a longer time period between images. However, the mapped regions in the image pair (contours in Figure 6c) show a very large additional acceleration of the glacier, roughly 2.5 times the previously mapped flow speed, i.e., an increase of 900 to 1250 ma^{-1}. The 2006 mapping also shows a step in the velocity field, rising from 1400 to 1600 ma^{-1} in less than 1 km, at a location near the upper part of the elevation loss anomaly. Differencing the two velocity fields (contours in Figure 6d) indicates that the largest flow speed increases occur on the flanks of the glacier, suggesting that the shear margins (the southern side in particular) have narrowed. Flow speed increased by up to a factor of 4 in that area by mid-2006.

4 Discussion

The highly localized nature of the elevation drawdown (Figure 3), and the short temporal duration of the anomalous elevation change event (Figure 2), and the marked change in the along flow profile (Figure 4) lead us to conclude that the primary cause of the anomalous (greater than adjacent areas) elevation change at the central Crane Glacier site was drainage of a kilometer-scale, relatively deep sub-glacial lake. The lake drainage period was between September 2004 and January 2006. Water depth drained from the sub-glacial reservoir was likely several tens of meters. This sub-glacial lake appears to be in one of a series of sub-glacial lake basins in the Crane Glacier fjord, as revealed by the bathymetry of Mueller et al. (2006) and Rebesco et al. (2010, submitted; Figure 1).

Other potential explanations, related to the rapidly changing ice dynamics of Crane Glacier after the loss of the Larsen B Ice Shelf, are not able to fully account for the magnitude and localization of elevation loss over the feature (e.g., Vieli and Nick, 2009). Recent ice models of Crane Glacier's post ice-shelf-loss responses do not show the anomaly, although they do adequately capture the changes in ice flow and

broader changes in thickness and elevation elsewhere along the glacier (Hulbe et al., 2008; Vieli et al., 2009).

Estimating the size of the Crane subglacial lake is difficult. Sergienko et al. 2007, showed that ice flow dynamics modify the surface expression of sub-glacial lake drainage, making it impossible to extract lake shape, size and volume from surface-measurable parameters. This is especially true in cases where the horizontal lake size is comparable to ice thickness. This appears to be the case for Crane Glacier, where ice thickness is of the order of 1000 m in the lower glacier trunk, and surface expression of the lake extends over 4.5 km along-flow and 2.2 km across-flow. In the Sergienko et al. model, moreover, it is shown that surface expression of lake drainage can be much larger than the area of the lake, especially along-flow, and that net surface lowering can be significantly less (in their modeled case, roughly 1/3) than the actual depth of subglacial lake level drainage.

Given this, and in the absence of reliable data on ice thickness and bedrock shape, we can only make arbitrary, approximate estimates of the size and depth of the inferred Crane sub-glacial lake feature. In Figures 3 and 4 we note both the limit of significant surface drawdown anomaly (4.5 by 2.2 km) and in Figure 3 we mark the region of maximum gradient in the anomaly boundary (1.9 by 1.5 km). Assuming this smaller region is the approximate extent of the lake, and that water depth was on the order of 100 m (and therefore a volume of about 0.2 km^3), we can explore the significance of the surface slope changes on the upper boundary of the lake, and the events leading to sudden drainage.

If the subglacier lake pressure is equilibrated with the overburden of ice directly above it, the slope of the ice-water interface is governed by a simple relationship related to the ice surface slope (i.e. the change in overlying ice thickness with horizontal distance) and the densities of ice and water:

$$\alpha_{water} = - \alpha_{ice} * (\rho_{ice} / \rho_{water} - \rho_{ice})$$

where α is slope and ρ is density for the respective materials (from Patterson, 1994). Because surface slope changes with time across the elevation anomaly region, there is a change in the ice/water slope of the upper lake surface. In fact, the change in upper surface of the lake would be a factor of 11 greater than the ice surface slope change, and in the opposite direction, if the water surface was in equilibrium everywhere with the local ice overburden.

Given the slope values in the table inset in Figure 4, and our approximation of lake size, this implies that the initial, pre-ice-shelf break-up lake surface had approximately 420 m relief (November 2001: 1.9 km * 0.020 * 11), rising from downstream to upstream. At the time of drainage, this would have increased to 690 m (November 2004: 1.9 km * 0.033 * 11). While it is unlikely that the ice above this lake was in full floatation equilibrium (Sergienko et al., 2007), this illustrates that a surface slope change across a subglacially trapped water body has a large effect on its geometry.

As Crane Glacier's slope steepened in response to loss of the ice shelf, the ice-water interface of the sub-glacial water body was tilted, raising the water level at the downstream boundary of the lake – i.e., at the obstruction to water flow that caused the lake. In our proposed scenario, the water level is raised until the obstruction is breached. The overlying ice was locally floated (i.e., hydraulically lifted) off the bedrock surface, and the lake volume was reduced by drainage. The dam may have been eroded by the drainage, or short-term details of the ice surface slope changes during drainage (e.g., a brief period of further steepening that is not captured by the series of profiles in Figure 4) pushed ~0.2 km^3 of water over the dam.

The Crane Glacier dynamics-driven lake drainage process brings up an important consideration for a feedback for climate-driven outlet glacier changes. This process is likely to be applicable to *any* glacier with ponded sub-glacial water bodies, when the glacier is undergoing rapid dynamic changes, and therefore rapid surface slope

changes. It is reasonable to suppose that many fjord-confined outlet glaciers have stable water bodies beneath them. In particular, the kinds of changes associated with climate warming (e.g., changes in the floating ice front, loss of contact with pinning points, loss of an ice shelf, or increased calving) accelerate the glacier, steepen its slope, and thereby disturb these water bodies in the sub-glacial bed, pushing the water into the sub-glacial system and thus reducing the basal shear stress (e.g., Clarke, 2005). As such, the drainage events may have a feedback effect on the glacier, causing a further acceleration in the system. Such a situation would pose a challenge for modeling of ice sheet response to climate and ocean warming.

However, our study of the ice flow speed change before and after the event (Figure 6) show that, in this case and perhaps generally, sub-glacial water drainage and movement produces relatively small changes in glacier speed, when compared to those caused by ice front retreat, or interactions with sub-glacial ridges or ice shelves. Overall, this pattern of rapid speed increase and slower decline, both in relative magnitude and in timing, matches the response characteristics of the similarly sized southeast Greenland glaciers, Helheim and Kangerdlugssuaq (compare Figure 5 to Howat et al., 2007; Nick et al., 2009) as their dynamics changed due to ice front retreats.

The Crane Glacier case here offers an opportunity to test the relative impact of two near-simultaneous events: ice front retreat from a bedrock ridge, and the drainage of a significant volume of water at mid-trunk, both initiated in late 2004. In Figure 6 the ice speed contours and speed difference contours show that the far greater effect is a general acceleration of the entire lower trunk (Figure 6c and 6d contours), both above and below the location of the lake. The dramatic crevasse pattern changes confirm this, and extend across and upstream of the inferred lake area. Small features in the contours near the upstream end of the lake indicated about a 20% net effect on flow speed change that may be associated with the sub-glacial lake drainage.

5 Conclusions

A rapid, localized elevation change in the lower central portion of Crane Glacier appears to be a result of sub-glacial lake drainage of a previously unknown lake beneath it. Bathymetry of the fjord, and sediments in basins within the newly-opened fjord, suggest that the new lake is one of a former series of subglacial water bodies. The Crane Glacier sub-glacial lake drainage was apparently triggered by surface slope changes along the glacier centerline during glacier retreat (Figure 4). Specifically, the retreat of the ice front from the sub-glacial ridge near 62.28° W longitude in late 2004 (Figure 1), appears to have caused a final further change in surface slope, that initiated rapid water discharge from the sub-glacial reservoir.

The pattern of ice speed change, both temporally and spatially, supports the idea that glacier interaction with sub-glacial fjord topography and ice front retreat across bedrock highs are the dominant control on ice flow and mass flux in outlet glaciers, and that sub-glacial water is of secondary importance. This high level of response to retreat from bedrock or pinning point features has been identified for tidewater outlet glaciers everywhere (Meier and Post, 1987; Howat et al., 2007; Howat et al., 2009; Joughin et al., 2003, Nick et al., 2009, Jenkins et al., 2010). Conversely, sub-glacial hydrologic changes, even significant ones, are at most (to date) a 20% effect on outlet glacier speed. (Stearns et al., 2008; Joughin et al., 2008; Zwally et al. 2002).

Acknowledgements

This research was supported by NASA grant NNG05GO82G to T. Scambos. E. Berthier acknowledges support from the French Space Agency (CNES) through the TOSCA and ISIS proposal #352. SPOT-5 HRS data were provided at no cost by CNES through the SPIRIT International Polar Year project (Korona et al., 2009). ASTER data were provided at no cost by NASA/USGS through the Global Land Ice Measurements from Space (GLIMS) project (Raup et al., 2007). Formosat-2 data used in the study (Figure 5) was acquired by the National Space Projects Office (NSPO) of Taiwan, and processed by Dr. Chien-Cheng Liu of National Cheng-Kung University in Tainan. We thank Jennifer Bohlander and Terry Haran of NSIDC, who produced several of the data sets used in the study.

References

Abdalati, W. and W. B. Krabill. 1999. Calculation of ice velocities in the Jakobshavn Isbrae area using airborne laser altimetry. *Remote Sens. Env.,* **67**(2), 194-204.

Bell, R. E., M. Studinger, C. A. Shuman, M. A. Fahnestock, and I. Joughin. 2006. Large subglacial lakes in East Antarctica at the onset of fast-flowing ice streams. *Nature,* **445**, 904-907.

Berthier, E., H. Vadon, D. Baratoux, Y. Arnaud, C. Vincent, K. L. Feigl, F. Remy, and B. Legresy. 2005. Surface motion of mountain glaciers derived from satellite optical imagery. *Remote Sens. Env.*, **95(1)**, 14-28.

Berthier, E., and T. Toutin. 2008. SPOT5-HRS digital elevation models and the monitoring of glacier elevation changes in North-West Canada and South-East Alaska, *Remote Sens. Env.*, **112**(5), 2443-2454.

Berthier, E., E. Schiefer, G. K. C. Clarke, B. Menounos, and F. Remy. 2010. Contribution of Alaskan glaciers to sea level rise derived from satellite imagery, *Nature Geosci.*, **3**(2), 92-95.

Bindschadler, R.A., and T.A. Scambos. 1991. Satellite-image-derived velocity field for an Antarctic ice stream. *Science*, **252**, 242-246.

Bo, S., M. J. Siegert, S. M. Mudd, D. Sugden, S. Fujita, C. Xiangbin, J. Yunyun, T. Xueyuan, and L. Yuansheng. 2009. The Gamburtsev mountiains and the origin and early evoution of the Antarctic Ice Sheet. *Nature,* **459**, 690-693.

Bouillon, A., M. Bernard, P. Gigord, A. Orsoni, V. Rudowski, and A. Baudoin. 2006. SPOT 5 HRS geometric performances: Using block adjustment as a key issue to

improve quality of DEM generation, *ISPRS Jour. of Photogrammetry and Remote Sens.*, **60**(3), 134-146.

Clarke, G. K. C. 2005. Subglacial processes. *Ann. Rev. Earth Sci.* **33**, 247-276, doi:10.1146/annurev.earth.33.092203.1222621.

Fricker, H. A., T. Scambos, R. Bindschadler and L. Padman. 2007. An active subglacial water system in West Antarctica mapped from space. *Science*, **315**, 1544-1548.

Fricker, H. A., and T. A. Scambos. 2009. Connected sub-glacial lake activity on lower Mercer and Whillans Ice Streams, West Antarctica 2003-2008. *J. Glaciol*. **55**(190), doi: 303-315.

Fujisada, H., G. B. Bailey, G. G. Kelly, S. Hara, and M. J. Abrams. 2005. ASTER DEM performance, *IEEE T Geosci. Remote Sens.*, **43**(12), 2707-2714.

Gray. L., I. Joughin, S. Tulaczyk, V. Spikes, R. Bindschadler and K. Jezek. 2005. Evidence for subglacial water transport in the West Antarctic Ice Sheet through three dimensional satellite radar interferometry. *Geophys. Res. Lett.*, **32**, L03501, doi: 10.1029/2004GL021387.

Howat, I., I. Joughin, and T. Scambos. 2007. Rapid changes in ice discharge from Greenland outlet glaciers. *Science*, **315**, doi:10.1126/science.1138478, 1559-1561.

Hulbe, C. L., T. A. Scambos, T. Youngberg, and A. K. Lamb. 2008. Patterns of glacier response to disintegration of the Larsen B ice shelf, Antarctic Peninsula. *Global and Planetary Change*, **63**(1), 1-8.

Jenkins, A., P. Dutrieux, S. S. Jacobs, S. D. McPhail, J. R. Perrett, A. T. Webb, and D. White. 2010. Observations beneath Pine Island Glacier in West Antarctica and implications for its retreat, *Nature Geosci*. **3**, 468-472.

Joughin, I., S. Das, M. King, B. Smith, I. M. Howat, and T. Moon. 2008. Seasonal speed-up along the western flank of the Greenland Ice Sheet. *Science* **320**(5877), 781-783, doi: 10.1126/science.1153288.

Korona, J., E. Berthier, M. Bernard, F. Remy, and E. Thouvenot. 2009. SPIRIT: SPOT 5 stereoscopic survey of Polar Ice: Reference Images and Topographies during the fourth International Polar Year (2007-2009), *ISPRS Journal of Photogrammetry & Remote Sensing*, **64**, 204-212.

Krabill, W. B., R. H. Thomas, C. F. Martin, R. N. Swift, and E. B. Fredrick. 1995. Accuracy of airborne laser altimetry over the Greenland ice sheet. *Int. J. of Remt. Sensing* **16**(7), doi:10.1080/01431169508954472, p. 1211-1222.

Meier, M. F., and A. Post. 1987. Fast tidewater glaciers. *Jour. Geophys. Res.*, **92**(B9), 9051-9058.

Mueller, R. D., L. Padman, E. Domack, B. Huber, V. Wilmott, A. Leventer, and S. Brachfield. 2006. Ocean/ice-shelf interactions around collapsing Antarctic Peninsula Ice Shelves. *Eos Trans. AGU*, **87**(52), Fall Meeting Suppl., Abstract C41C-0346.

Nick, F. M., A. Vieli, I. M. Howat, and I. Joughin. 2009. Large-scale changes in Greenland outlet glacier dynamics triggered at the terminus, *Nature Geosci*., **2**(2), 110-114.

Paterson, W. S. B. 1994. *The Physics of Glaciers, 3rd Edition.* Pergamon, Great Britain, 480 pp.

Pattyn, F. 2010. Antarctic subglacial conditions inferred from a hybrid ice sheet–ice stream model. *Earth Planet. Sci. Lett.,* **295**, 451-461, doi:10.1016/j.epsl.2010.04.025.

Rack, W., and H. Rott. 2004. Pattern of retreat and disintegration of the Larsen B ice shelf, Antarctic Peninsula. *Ann. Glaciol.* **39**(1), 505-510.

Raup, B., A. Kääb, J. S. Kargel, M. P. Bishop, G. Hamilton, E. Lee, F. Paul, F. Rau, D. Soltesz, S. J. S. Khalsa, M. Beedle, and C. Helm. 2007. Remote sensing and GIS technology in the Global Land Ice Measurements from Space (GLIMS) project, *Computers & Geosciences*, **33**(1), 104-125.

Rebesco, M., F. Zgur, E. Domack, A. Leventer, S. Brachfeld, V. Wilmott, A. DeMoor, and G. Halverson. 2010, submitted. Evolution of grouding line systems following collapse of the Larsen B Ice Shelf, Antarctica. Submitted to *Science*.

Remy, F., and B. Legresy. 2004. Subglacial hydrological networks in Antarctica and their impact on ice flow, *Ann. Glaciol.* **39**, 67-72.

Rignot, E., G. Casassa, P. Gogineni, W. Krabill, A. Rivera, and R. Thomas. 2004. Accelerated ice discharge from the Antarctic Peninsula following the collapse of Larsen B ice shelf. *Geophys. Res. Lett.,* **31**, L18401, doi:10.1029/2004GL020697.

Scambos, T. A., M. J. Dutkiewitcz, J. C. Wilson, and R. A. Bindschadler. 1992. Application of image cross-correlation software to the measurement of glacier velocity using satellite image data. *Remt. Sensing Env*., **42**, 177-186.

Scambos, T. A., J. Bohlander, C. Shuman, and P. Skvarca. 2004. Glacier acceleration and thinning after ice shelf collapse in the Larsen B embayment, Antarctica. *Geophys. Res. Lett.*, **31**, L18402, doi: 10.1029/2004GL020670.

Scambos, T., and C.-C. Liu. 2009. A closer look at polar ice: Formosat-2 and glacier changes in the Arctic and Antarctic. *Proceedings of the Formosat-2 5th Anniversary Conference*, Hshinchu, Taiwan, 19-21 May, 2009.

Sergienko, O. D. R. MacAyeal and R. A. Bindschadler. 2007. Causes of sudden, short-term changes in ice-stream surface elevation. *Geophys. Res. Lett.*, **33**, L22503, doi:10.1029/2007GL031775.

Shabtaie, S. and C. R. Bentley, 1988. Ice thickness map of West Antarctic Ice Streams by radar sounding. *Ann. Glaciol.* **11**, 126-136.

Shuman, C. A., H.J. Zwally, B.E. Schutz, A.C. Brenner, J.P. DiMarzio, V.P. Suchdeo and H.A. Fricker. 2006. ICESat Antarctic elevation data: preliminary precision and accuracy assessment, *Geophys. Res. Lett.*, **33**, L07501, doi:10.1029/2005GL025227.

Shuman, C. A., E. Berthier, and T. Scambos. 2010. Multi-sensor assessment of Larsen B tributary glacier elevations, 2003-2009, Antarctic Peninsula. *J. Glaciol.,* submitted.

Shutz, R., J. Zwally, C. Shuman, D. Hancock, and J. DiMarzio. 2005. Overview of the ICESat Mission. *Geophys. Res. Lett.*, **32**, L21S01, doi:10.1029/2005GL024009.

Siegert, M., S. Carter, I. Tabacco, S. Popov, and D. D. Blakenship. 2005. A revised inventory of Antarctic subglacial lakes. *Antarctic Science* **17**(3), 453-460, doi:10.1017/S0954102005002889.

Smith, B. E., H. A. Fricker, I. R. Joughin, and S. Tulaczyk. 2009. An inventory of subglacial lakes in Antarctica detected by ICESat (2003-2008). *J. Glaciol*. **55**(192), 573-595, doi:10.3189/002214309789470879.

Stearns, L. A., B. E. Smith, and G. S. Hamilton. 2008. Increased flow speed on a large East Antarctic glacier caused by subglacial floods. *Nature Geosci*., **1**, 827-831, doi:10.1038/ngeo356.

Toutin, T. 2008. ASTER DEMs for geomatic and geoscientific applications: a review. *Int. Jour. Remt. Sens.*, **29**(7), 1855 - 1875.

van de Wal, R. S. W., W. Boot, M. R. van den Broeke, C. Smeets, C. H. Reijmer, J. J. A. Donker, and J. Oerlemans. 2008. Large and rapid melt-induced velocity changes in the ablation zone of the Greenland Ice Sheet. *Science*, **321**(5885), 111-113.

Vaughan, D. G., H. F. J. Corr, F. Ferraccioli, N. Frearson, A. O'Hare, D. Mach, J. Holt, and others, 2006. New boundary conditions for the West Antarctic Ice Sheet: subglacial topography beneath Pine Island Glacier. *Geophys. Res. Lett*., **33**, L09501. doi:10.1029/2005GL025588.

Vieli, A., and F. Nick. 2009. Understanding dynamic changes of marine terminating outlet glaciers through combining observations and numerical modeling: the case of Crane Glacier, Antarctic Peninsula. *Eos Trans. AGU* **90**(52), Fall Meeting Suppl., Abstract C13A-06.

Wingham, D. J., M. J. Siegert, A. Shepherd, and A. S. Muir. 2006. Rapid discharge connects Antarctic sub-glacial lakes. *Nature*, **440**(20), doi:10.1038/nature04660.

Zwally, H. J., R. Shutz, W. Abdalati, and six others. 2002. ICESat's laser measurements of polar ice, atmosphere, ocean, and land. *J. Geodynamics*, **34** (3-4), 405-445.

Zwally, H. J., W. Abdalati, T. Herring, K. Larson, J. Saba, and K. Steffen. 2002. Surface melt-induced acceleration of Greenland ice sheet flow. *Science* **297**(5579), 218-222, doi:10.126/science.1072708.

Tables

Table 1. Satellite images and image pairs used for elevation and velocity measurement

Sensor	Band	Date acquired	Resolution	Vel Error	Fig. 3	Fig. 4	Fig. 5	Fig. 6
ASTER	1	22 Nov 2001	15 m			*		
ASTER	1	07 Nov 2002	15 m		*			
Landsat 7 ETM+	8	06 Apr 2002	15 m	±16 ma^{-1}			*	
Landsat 7 ETM+	8	18 Dec 2002	15 m				*	
Landsat 7 ETM+	8	18 Dec 2002	15 m	±64 ma^{-1}			*	*
Landsat 7 ETM+	8	20 Feb 2003	15 m				*	*
Landsat 7 ETM+	8	20 Feb 2003	15 m	±13 ma^{-1}			*	
ASTER	1	13 Jan 2004	15 m			*	*	
ASTER	1	27 Sep 2004	15 m		*	*		
SPOT5	Pan	01 Jan 2006	10 m	± 8 ma^{-1}	*	*	*	*
SPOT5	Pan	25 Nov 2006	10 m		*	*	*	*
Formosat-2	Pan	11 Feb 2008	2 m	± 3 ma^{-1}			*	
Formosat-2	Pan	14 Mar 2009	2 m				*	
SPOT5	Pan	24 Dec 2009	2.5 m	± 5 ma^{-1}			*	
SPOT5	Pan	09 Jan 2010	2.5 m				*	

Figure captions

Figure 1. Satellite image map of lower Crane Glacier and fjord. Inset, locator map of Crane Glacier, within the Larsen B embayment, Antarctic Peninsula; major ice shelf break-up events for the region are mapped. Main image is from SPOT-5 HRS sensor, acquired 25 November 2006. Recent airborne laser altimetry tracks (ATM: 2002, 2004, and 2008 in yellow, orange, and red respectively) and satellite laser altimetry tracks (ICESat: 2003-2009, straight green line) show significant elevation changes on the glacier, which are anomalously large in the irregular region at their intersection (interpreted in this study as resulting from a sub-glacial lake). Bathymetric contours of the fjord are from multi-beam sonar mapping in 2006 (E. Domack, pers. comm., and Rebesco et al., 2010 in press). Numbers in the fjord (1, 2, and 3) and dashed outlines represent flat sediment-filled basins interpreted as past sub-glacial lake deposits. Grounding line of 1998-2002 is from SAR interferometry (Rack and Rott, 2004). Ice front locations for floating (Nov. 2002) and grounded ice

fronts are shown; since Nov. 2006 the ice front position has been essentially unchanged. Figure 2. Elevation change versus time at the intersection of ICESat-1 track 0018 and the ATM laser altimetry ground tracks, near the center of lower Crane Glacier. The elevation datum is the WGS-84 ellipsoid.

Figure 3. Elevation change from satellite-image stereo-pair DEM differencing over lower Crane Glacier. Main panel, DEM difference between ASTER image-derived DEMs acquired 27 September 2004 and SPOT-5 SPIRIT data acquired 01 January 2006. Dashed black outline indicates the limit of anomalous elevation loss from satellite and aircraft altimetry profiles; solid black outline marks the approximate largest gradient in the difference DEM for the region. Inset, SPOT-5 DEM difference of the same area for DEMs acquired 01 January 2006 and 25 November 2006. White dashed line is for reference. Elevation change scale is the same for both panels; mottled blue and pale brown areas are mountainous regions flanking the glacier.

Figure 4. Along-flow elevation profiles from ATM and satellite stereo-image DEMs for the lower Crane Glacier, 2001 - 2008. Red -blue line pairs for ATM data show the range of elevation variation across the swath of ATM laser measurements. Slope values in the inset table are the mean slope for a 4.51 km region defined by the difference of the November 2002 and January 2006 elevation profiles (lower left inset). Note that the ATM 2008 (asterisked) value is derived from a profile that deviated from the centerline significantly (see Figure 1).

Figure 5. Elevation changes as in Figure 2, with flow speed changes over time superimposed (right-hand scale). Mean ice speed of the area at the intersection of ICESat-1 Track 0018 and the ATM profiles (Figure 1) was determined from image pair velocity mapping (see Table 1). Horizontal bars for speed determinations represent the time between the image pair acquisitions. Errors in the speed determination are within the symbol size (<30 m/yr) except for the December 2002 - February 2003 pair (± 64 m/yr).

Figure 6. ASTER (a and b) and SPOT5 (c and d) image series showing crevasse changes in the lower Crane Glacier spanning the period of inferred lake drainage, i.e. between scene b and c. Superimposed on image d are contours of flow speed difference between ice speed maps of the lower trunk using Dec. 2002 - Feb. 2003, and Jan. 2006 - Nov. 2006 image pairs (see Table 1). SPOT5 images copyright CNES/ distribution by Spot Image, SPIRIT project.

Figure 7. Conceptual model of the sub-glacial drainage event. The downstream obstruction is represented by the large vertical bar. This may be eroded or fractured by water flow during drainage (lower panel).

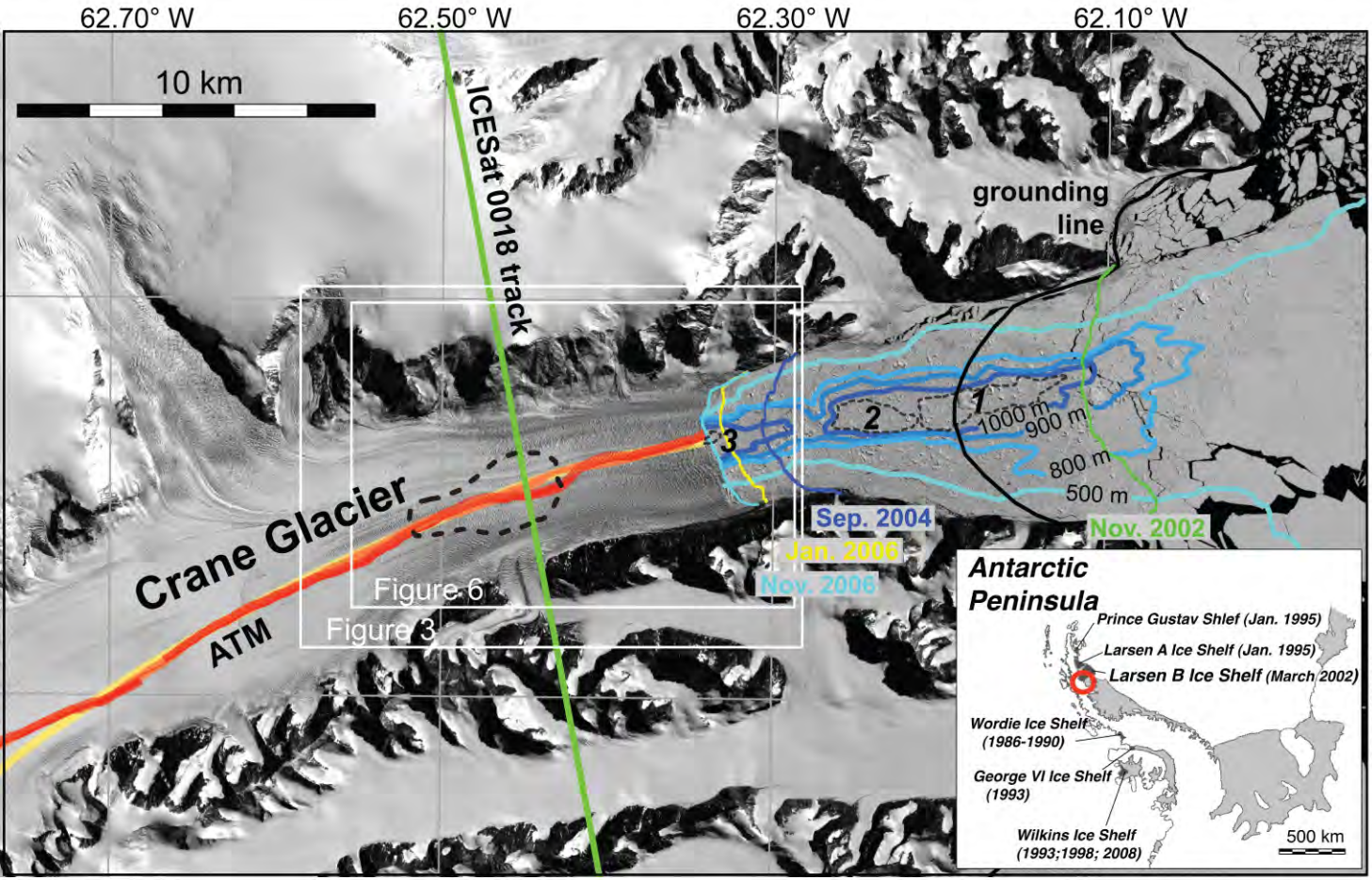

Figure 1 Scambos et al.
B/W, print at 85% scale.

Figure 1. Satellite image map of lower Crane Glacier and fjord. Inset, locator map of Crane Glacier, within the Larsen B embayment, Antarctic Peninsula; major ice shelf break-up events for the region are mapped. Main image is from SPOT-5 HRS sensor, acquired 25 November 2006. Recent airborne laser altimetry tracks (ATM: 2002, 2004, and 2008 in yellow, orange, and red respectively) and satellite laser altimetry tracks (ICESat: 2003-2009, straight green line) show significant elevation changes on the glacier, which are anomalously large in the irregular region at their intersection (interpreted in this study as resulting from a sub-glacial lake). Bathymetric contours of the fjord are from multi-beam sonar mapping in 2006 (E. Domack, pers. comm., and Rebesco et al., 2010 in press). Numbers in the fjord (1, 2, and 3) and dashed outlines represent flat sediment-filled basins interpreted as past sub-glacial lake deposits. Grounding line of 1998-2002 is from SAR interferometry (Rack and Rott, 2004). Ice front locations for floating (Nov. 2002) and grounded ice fronts are shown; since Nov. 2006 the ice front position has been essentially unchanged.

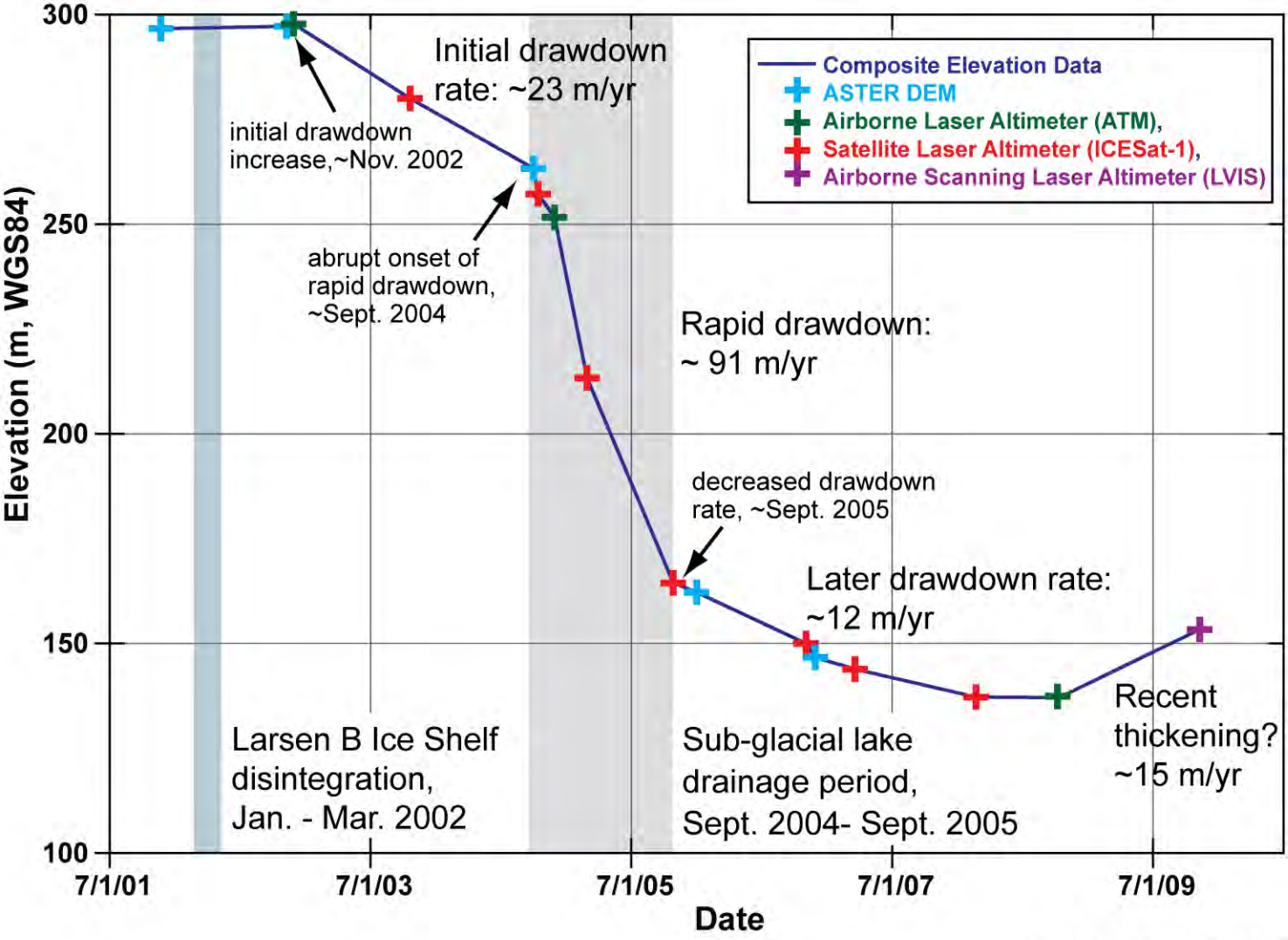

Figure 2 Scambos et al.
B/W, print at 50% scale.

Figure 2. Elevation change versus time at the intersection of ICESat-1 track 0018 and the ATM laser altimetry ground tracks, near the center of lower Crane Glacier.

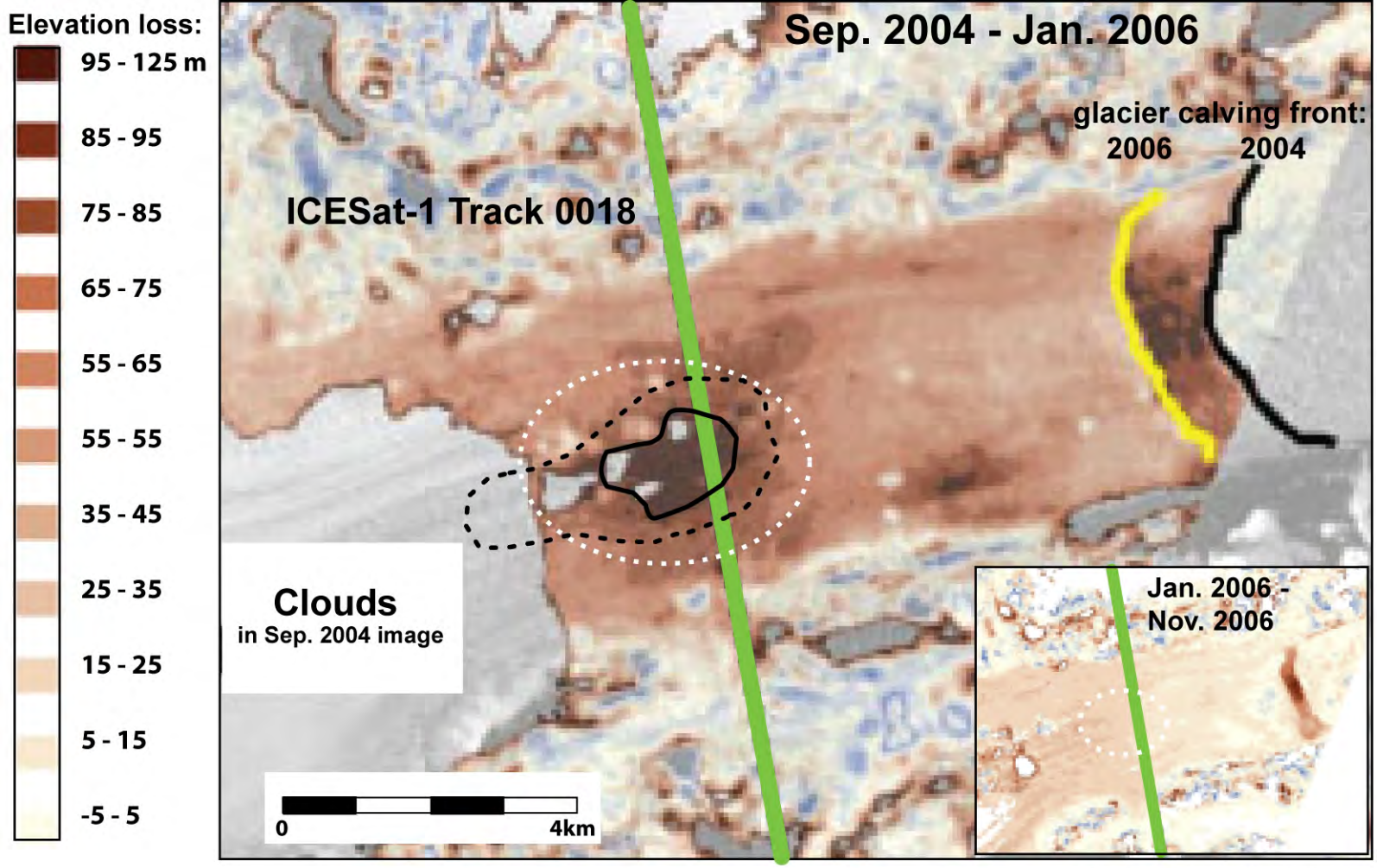

Figure 3 Scambos et al.
Color, print at 50% scale.

Figure 3. Elevation change from satellite-image stereo-pair DEM differencing over lower Crane Glacier. Main panel, DEM difference between ASTER image-derived DEMs acquired 27 September 2004 and SPOT-5 SPIRIT data acquired 01 January 2006. Dashed black outline indicates the limit of anomalous elevation loss from satellite and aircraft altimetry profiles; solid black outline marks the approximate largest gradient in the difference DEM for the region. Inset, SPOT-5 DEM difference of the same area for DEMs acquired 01 January 2006 and 25 November 2006. White dashed line is for reference. Elevation change scale is the same for both panels; mottled blue and pale brown areas are mountainous regions flanking the glacier.

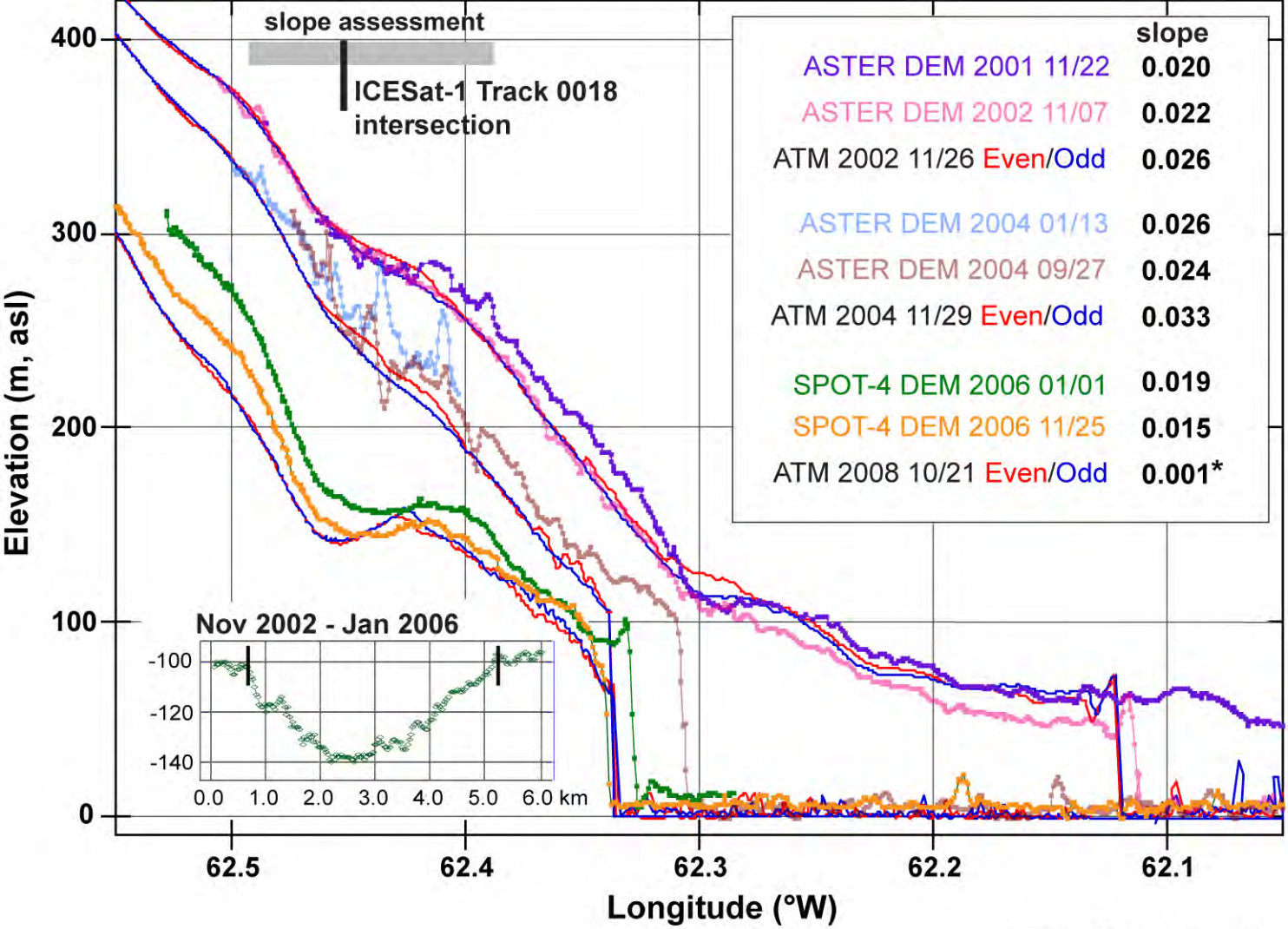

Figure 4 Scambos et al.
Color, print at 80% scale.

Figure 4. Along-flow elevation profiles from ATM and satellite stereo-image DEMs for the lower Crane Glacier, 2001 - 2008. Red -blue line pairs for ATM data show the range of elevation variation across the swath of ATM laser measurements. Slope values are the mean slope for a 4.51 km region defined by the difference of the November 2002 and January 2006 elevation profiles (inset). Note that the ATM 2008 (asterisked) value is derived a profile that deviated from the centerline significantly (see Figure 1).

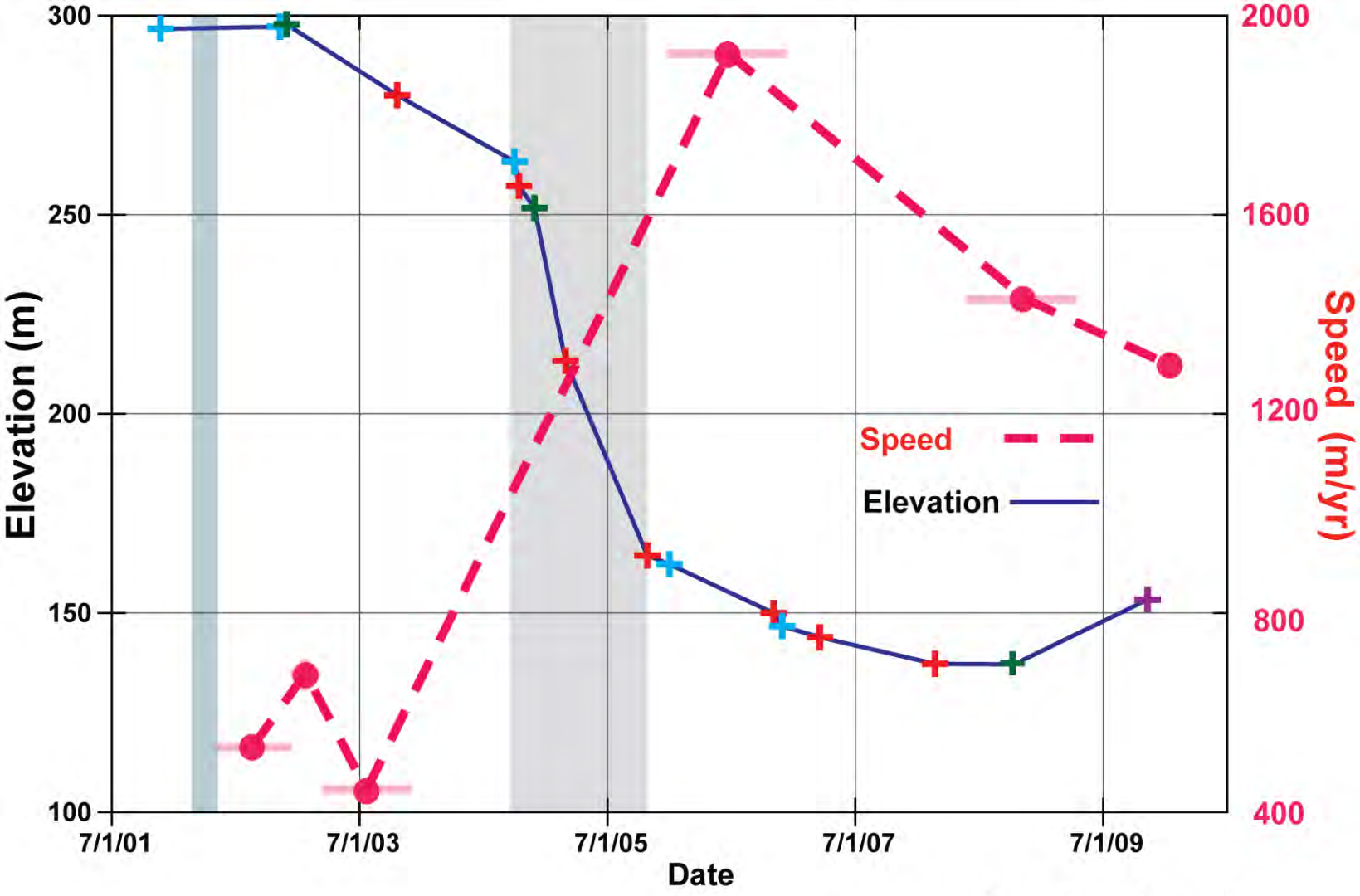

Figure 5 Scambos et al.
B/W, print at 50% scale.

Figure 5. Elevation changes as in Figure 2, with flow speed changes over time superimposed (right-hand scale). Mean ice speeds of a 3 km^2 area at the intersection of ICESat-1 Track 0018 and the ATM profiles (Figure 1) were determined from image pair velocity mapping (see Table 1). Horizontal bars for speed determinations represent the time between the image pair acquisitions. Errors in the speed determination are within the symbol size (<30 m/yr) except for the December 2002 - February 2003 pair (± 60 m/yr).

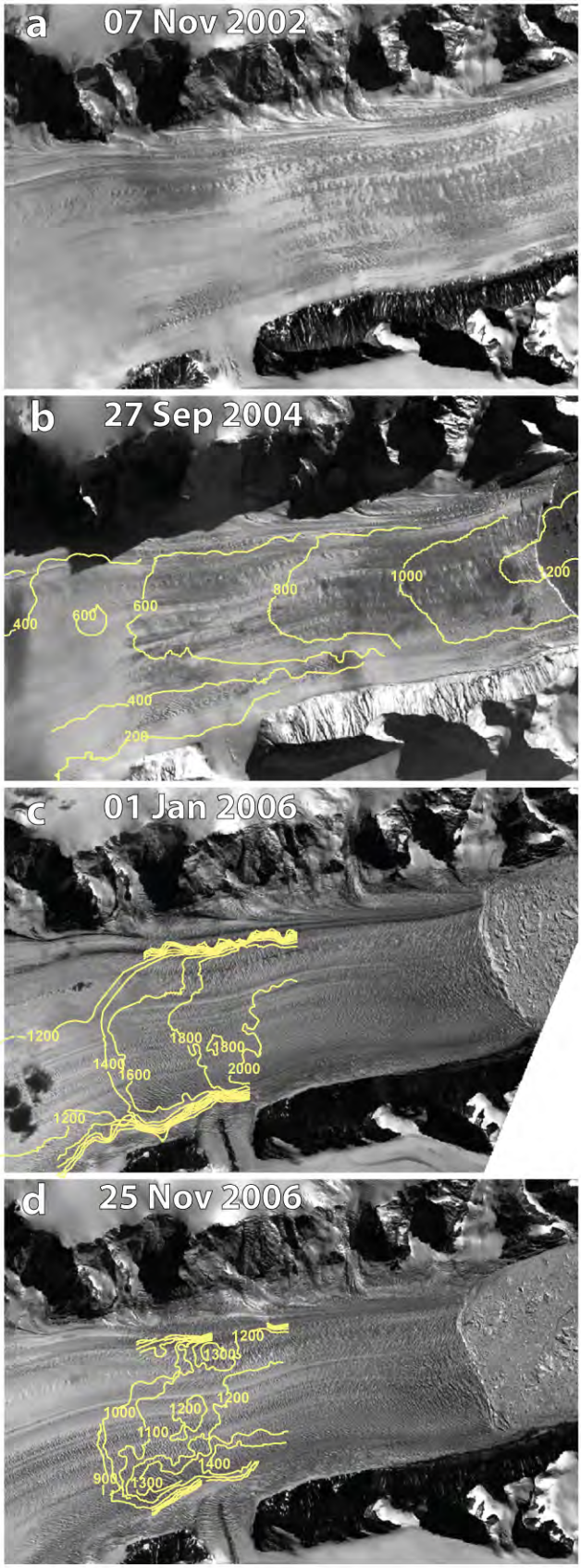

Figure 6 Scambos et al. color print at this scale.

Figure 6. ASTER (a and b) and SPOT-5 (c and d) image series showingcrevasse changes in the lower Crane Glacier spanning the period of inferred lake drainage, i.e. between scene b and c. Superimposed on image d are contours of flow speed *difference* between ice speed maps of the lower trunk using Dec. 2002 - Feb. 2003, and Jan. 2006 - Nov. 2006 image pairs (see Table 1). SPOT-5 images copyright CNES/ distribution by SPOT image, SPIRIT project.